Journal of Korean Association of Crystal Growth
Vol. 8, No. 3 (1998) 448-453

Gas phase temperature profile measurement of an upflow OMVPE reactor by laser Raman spectroscopy

Chinho Park and Timothy J. Anderson*

School of Chemical Engineering and Technology, Yeungnam University, Kyongsan 712-749, Korea
**Department of Chemical Engineering, University of Florida, Gainesville, FL 32611, U.S.A.*

레이저 라만 분광법을 이용한 도립형 OMVPE 반응기의 기상 온도 분포 측정

박진호, Timothy J. Anderson*

영남대학교 화학공학 및 공업화학부, 경산, 712-749
*플로리다대학교 화학공학과, 게인스빌, 플로리다, 미국 32611

Abstract An inverted, stagnation point flow OMVPE reactor was studied by laser Raman spectroscopy. Pure rotational Raman scattering by the carrier gas (N_2 or H_2) was used to determine the axial centerline temperature profile in the reactor as a function of the inlet flow velocity and the reactor aspect ratio. A larger temperature gradient normal to the susceptor surface was obtained with higher gas flow velocity, larger aspect ratio, and the use of a N_2 carrier gas.

요 약 도립형 OMVPE 반응기를 레이저 라만 분광법을 사용하여 조사하였다. 운반기체인 질소나 수소의 순수한 회전 라만 분산 스펙트럼을 통해 반응기 내부의 축 중심 방향의 온도 분포를 정확히 측정할 수 있었다. 주입 기체의 유속과 반응기의 종횡비가 변수로 변화되었으며 실험 결과, 기판 표면 근처의 수직방향 온도 구배를 크게 유지하기 위해서는 보다 빠른 기체 유속의 사용, 보다 큰 반응기 종횡비의 사용, 그리고 질소의 사용이 유리함을 알 수 있었다.

1. Introduction

Organometallic Vapor Phase Epitaxy (OMVPE) is a versatile technique for depositing epitaxial films of compound semiconductors and their alloys [1,2]. Since OMVPE reactors are usually operated in the mass transport limited regime, the quality and uniformity of the deposited layers are strongly influenced by the gas dynamics. It is desirable to establish a uniform flow field in the reactor that is free of laminar vortices to minimize the reactant switching time. Gas phase isotherms parallel to the substrate are also desirable to achieve uniform growth, and a large normal thermal gradient in the vicinity of the substrate minimizes parasitic gas phase reactions and reduces particle impingement rates. A large temperature gradient normal to the substrate surface can, however, lead to recirculation flow patterns in the reactor causing growth rate variations, delayed impurity incorporation, and graded heterojunctions [3]. These issues have been addressed in several modeling and experimental investigations [4-7] of conventional reactor geometries (e.g., horizontal, vertical downflow, and rotating disk configurations).

This study reports experimental temperature profile measurements of an unconventional upflow, stagnation-point reactor. With this configuration, a stabilizing density gradient is expected, thereby eliminating or reducing the flow recirculation effects frequently encountered in conventional geometries at otherwise similar operation conditions. In addition, particulate impingement effects should be reduced because of the favorable alignment of the reactor with respect to gravity. Wafer mounting onto the inverted susceptor, of course, would be more difficult than in the non-inverted designs.

Stagnation-point flow reactors have been investigated by several workers and their results have shown that the reactor orientation strongly affects

the extent of natural convection produced by thermal gradients in the gas phase [7-13]. Numerical calculations have suggested that natural convection driven cells can be reduced by increasing the inlet flow rate, rotating the susceptor, reducing the reactor pressure, reshaping the reactor wall, decreasing the distance between the inlet and the susceptor, introducing baffles, or inverting the reactor [5, 14, 15]. The characterization of an inverted vertical OMVPE reactor, however, has received little attention.

In this study, temperature distributions were measured in a vertical upflow OMVPE reactor by laser Raman spectroscopy. The axial centerline temperature profiles near the susceptor surface were measured by pure rotational Raman scattering from the carrier gas molecules, N_2 or H_2, as a function of the inlet flow velocity and aspect ratio, and the results were discussed.

2. Experimental Procedure

A schematic of the reactor geometry is shown in Fig. 1 along with its physical dimensions. A feature of the reactor is the provision of a sweeping gas flow to prevent wall deposition for studies involving organometallic precursors. The reactor body was made of optically flat quartz with a square cross-section to minimize the position-dependent intensity variations of the Raman signal due to irregular surface scattering. A cylindrical quartz tube was then inserted into the reactor to simulate a practical geometry and simplify the reactor model. Four vertical slits, each separated by 90°, were opened in this tube and were positioned symmetrically with respect to the axial centerline of the reactor. These slits permitted access by the laser beam to the reactor centerline and detection of the scattered light from the reactor. With this arrangement experimental temperature measurements could only be performed along the axial centerline of the reactor. The reactor bottom and top flanges were made of 316 stainless steel and contained recessed grooves (square) in which O-rings were placed to seal the quartz reactor.

A resistance heater assembly was inserted through the top plate of the reactor and served as the susceptor. The body of the furnace was a cylindrical quartz tube (3.8 cm O.D.), and a vacuum was maintained ($<10^{-3}$ torr) inside the quartz to insulate the heating block from the surroundings. The heating block made a physical contact with the inside bottom of the quartz furnace body. The set point temperature of the furnace was measured at the inside bottom wall of the furnace body by a type-K thermocouple, and the temperature was controlled at 650°C for all experiments. The details of the furnace design are described elsewhere [16].

The reactor aspect ratio (AR), which is defined as the ratio of the distance between the susceptor and the center inlet tube to the center tube diameter (3.8 cm), could be varied by moving the furnace assembly to achieve a maximum value of AR=2. The carrier gas, N_2 or H_2, was introduced into the reactor through the center and outer inlet tubes simultaneously. A straight tube was directly connected to the center inlet tube, and a second tube, formed in a spiral configuration, surrounded the inner inlet and the flat spiral was oriented parallel to the susceptor surface. The end of this latter tube was capped and several small holes were opened on the upper tube wall to provide a uniform sweeping flow around the center flow. Stainless steel meshes were placed on top of both inlet tubes which were packed with 3 mm diameter glass beads to provide a nearly flat velocity profile at each gas inlet. The entire reactor was situated in the macrochamber of the Raman system, and the reactor could be translated in three directions by a micrometer controlled x-y-z stage. The operating pressure of the reactor was maintained at atmospheric pressure.

A Ramanor U-1000 Raman spectrometer (ISA, Inc.) was used to collect and analyze the scattered light in a 90° configuration. The excitation laser beam was introduced in the -x direction (Fig. 1), and the scattered light was detected in the +y direction, forming a xy scattering plane. The 488 nm line of cw argon ion laser was used as the excitation source at a laser power of 1 W. Polarization of the incident laser was in the z direction, but the scattered light polarization was not analyzed in these experiments. A photomultiplier tube (PMT) was used as a detector, and photon counting electronics were employed.

The temperature distribution in the reactor was measured by collecting and analyzing the pure rotational Raman scattered light from the carrier gas molecules flowing in the reactor. This technique has the advantage of not disturbing the flow

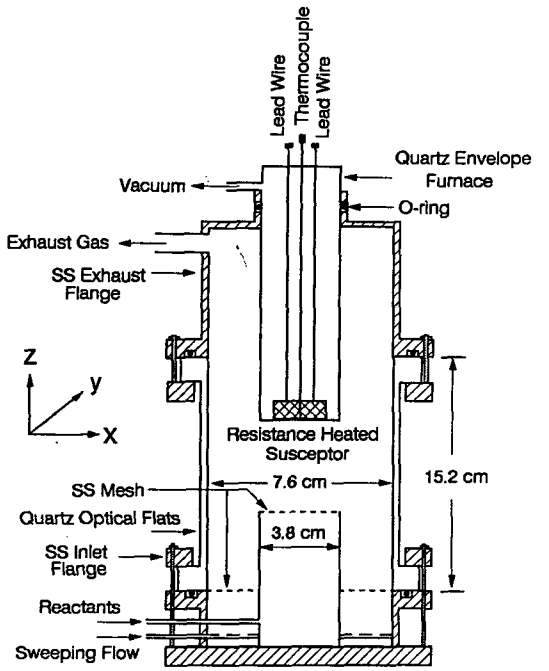

Fig. 1. Schematic of the experimental vertical upflow reactor.

field as compared to the use of a thermocouple [17], and it provides a spatial resolution in three dimensions better than interference holography [18]. In this study, spatial resolutions of about 30 μm in the y and z direction and about 3000 μm in the x direction could be obtained, where the values were calculated with the assumption of a focal cylinder [19]. In addition, measurements as close to the susceptor surface as 0.3 mm could be performed. The determination of the origin could be easily reproduced by monitoring the scattered light intensity decrease as the laser path intersected with the edge of the susceptor surface upon translation in the +z direction.

The theory of Raman scattering is very well developed for diatomic molecules [19]. Assuming thermal equilibrium for the rotational modes, the scattering intensities for rotational Raman scattering from an assembly of randomly oriented (e.g., gas) diatomic molecules can be described by explicit expressions [20]. The assumption of thermal equilibrium is reasonable in this study since both the temperature and pressure are high.

The Raman spectra were obtained with a resolution of 1.5 cm^{-1} and an integration time of 1 s. Spectrometer frequencies were calibrated by the neon emission line at 5400.6 Å. In the case of N_2, transitions from J=0 to 20 were clearly observed, where J represents the rotational quantum number of the initial level for the Stokes band and the final level for the anti-Stokes band. For N_2, the Stokes bands alone were sufficient to determine the temperature. For H_2, however, only four Stokes and two anti-Stokes bands had a sufficiently large signal-to-noise ratio to be useful. Thus all 6 bands were included in the analysis to determine the temperature.

The data obtained in this study showed the expected relationship, indicating that the assumption of a Boltzmann population of the occupied rotational energy levels was reasonable. The accuracy of the measured temperature depends on the signal-to-noise ratio which decreases with increasing temperature. When the furnace temperature was higher than 800℃, radiation from the heating block increased the noise level, especially when the laser probe was near the susceptor surface. At the furnace temperature of this study (650℃), the radiation was reduced, and the spectra obtained showed reasonable signal-to-noise ratios (>8:1). The uncertainty of the temperature, defined as one standard deviation, was calculated from the goodness-of-fit to the explicit expressions [20] and was less than ±20℃ for most measurements of this study. The temperature of N_2 was more accurately determined than that of H_2 because more data were available for N_2.

3. Results and Discussion

The axial centerline temperature profile in the reactor was measured for both N_2 and H_2 carrier gases as a function of the inlet gas flow velocity and the aspect ratio. Figure 2 shows the axial temperature profile in the reactor for both N_2 and H_2 carrier gases at the same operating conditions (i.e., a gas inlet velocity of 3.0 cm/s for both the center and the sweeping flows, AR=1, and 650℃ susceptor set point temperature). The lines shown in this figure are a spline interpolation of the data. These results clearly show that the use of a N_2 carrier gas produces a steeper temperature gradient normal to the susceptor surface than the use of a H_2 carrier gas. The same trend was obtained by other investigators using both horizontal [4, 6, 21-25] and

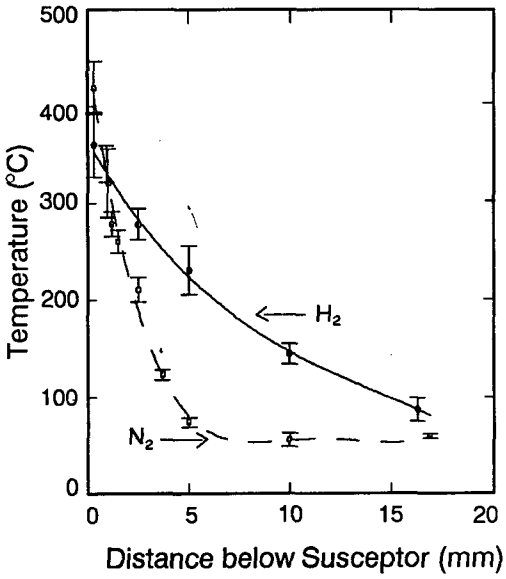

Fig. 2. Axial centerline temperature profile in the reactor for N_2 and H_2: AR=1, v_0=3.0 cm/s (center and sweeping), T_{set}=650°C.

vertical downflow [26, 27] reactor geometries. The result is easily understood by considering the nearly 8 times higher thermal conductivity of H_2 compared with that of N_2. As a result the N_2 temperature remains low in a large volume below the susceptor even for the low gas flow velocities used in this study.

The extrapolated susceptor surface temperature is considerably lower than the set point temperature (650°C) measured at the inside bottom wall of the furnace. This result suggests that a significant thermal contact resistance exists between the heating block and the inside wall of the quartz furnace housing. A similar phenomenon was observed by Koppitz et al. [21] using a heater design similar to the one of this study. Their data indicate a temperature difference between the susceptor surface and the susceptor control temperature of approximately 200°C with a set point temperature of 727°C using H_2 as the carrier gas. Monteil et al. [26], however, did not observe this large temperature difference, since they used a RF heated graphite susceptor with embedded thermocouples.

In another experiment using N_2 as the carrier gas, the susceptor surface temperature was measured by a thermocouple directly bonded to the susceptor outer surface using a ceramic epoxy. The thermocouple measured a surface temperature (370°C) even lower than the extrapolated surface temperature (460°C), consistent with a significant internal contact resistance and the additional thermocouple contact resistance and the conductive and convective heat losses along the thermocouple wire. These results emphasize the importance of calibrating the surface temperature, since the large deviation between the measured surface temperature and the control temperature can give difficulties in the interpretation of growth data and reproducibility.

The measured temperature profile when using N_2 as the carrier gas showed that the gas temperature approaches a constant value that is approximately 25°C higher than room temperature at distances greater than 17 mm from the susceptor. Presumably this was caused by radiation heating of the stainless steel center inlet tube and its packing material which preheated the inlet gas. It was not possible to measure the inlet temperature in the more conductive H_2 carrier gas because the system did not allow probing beyond 17 mm below the susceptor at AR=1.

The effect of changing the inlet gas velocity on the axial temperature profile in the reactor was investigated for both the N_2 (Fig. 3) and H_2 carrier gases (Fig. 4). As expected, increasing the inlet velocity resulted in a steeper temperature gradient as a result of the decreased residence time in the

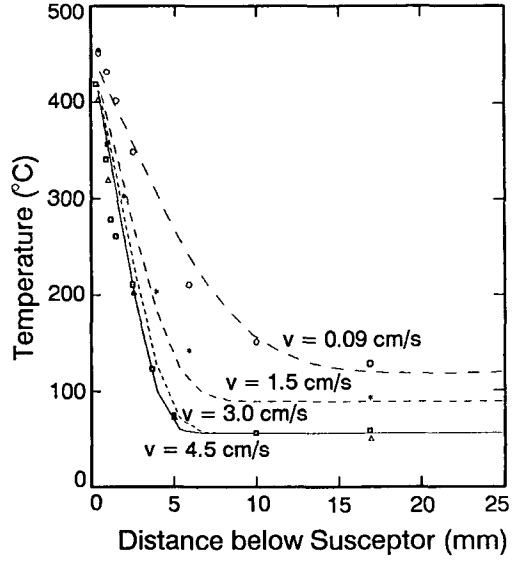

Fig. 3. The effect of varying the gas inlet velocity on the axial centerline temperature profile in the reactor for the N_2 carrier gas: AR=1, T_{set}=650°C.

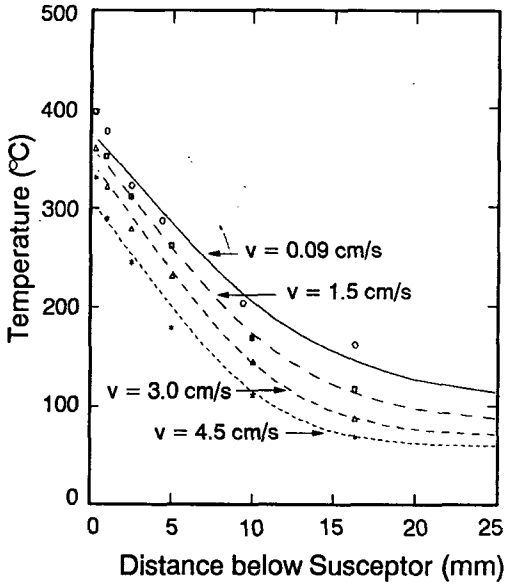

Fig. 4. The effect of varying the gas inlet velocity on the axial centerline temperature profile in the reactor for the H_2 carrier gas: AR=1, T_{set}=650°C.

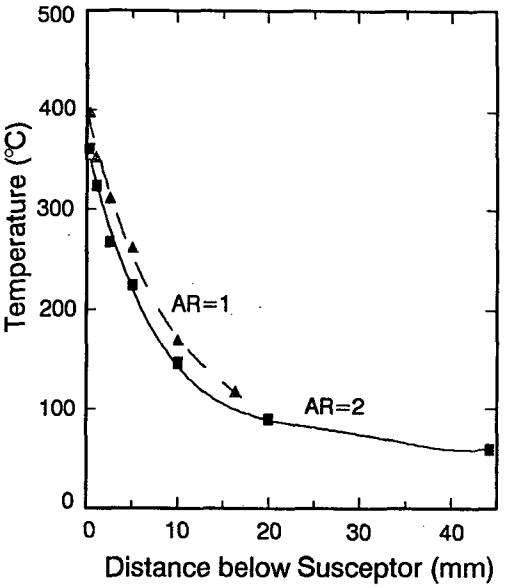

Fig. 5. The effect of varying the aspect ratio (AR) on the axial centerline temperature profile in the reactor for the H_2 carrier gas: v_0=1.5 cm/s (center and sweeping), T_{set}=650°C.

reactor with increased velocity. Cooling of the center tube was also enhanced with higher gas velocity. For inlet flow velocities greater than 3.0 cm/s, including measurements at 9.0 cm/s not shown in Fig. 3, the axial temperature profile did not change for the N_2 carrier gas. The high temperature zone (>200°C) was restricted to a region within 2.5 mm from the susceptor surface at these high velocities. This narrow high temperature zone near the susceptor was visually observed as a thin cloud of indium droplets when trimethyl indium was introduced into the center flow. In the case of the H_2 carrier gas, however, the temperature profile systematically varied in the velocity range studied (0.09 to 4.5 cm/s), with the axial temperature gradient increasing with increasing inlet flow velocity. The high temperature zone (>200°C) was confined to a region within 5 mm from the susceptor surface for H_2 carrier gas at the highest inlet flow velocity studied (4.5 cm/s).

The effect of changing the aspect ratio on the centerline temperature profile was investigated and the results are shown in Fig. 5 for H_2 carrier gas. Using a larger aspect ratio (AR=2) produced a slightly greater temperature gradient, and this is attributed to a decrease in radiation heating of the center tube from the hot susceptor. A decrease in the temperature near the center inlet tube was observed with increasing aspect ratio. The shift in the temperature profile produced by increasing the aspect ratio, however, was not large at the operating conditions examined in this study.

From the viewpoint of the gas dynamics, the use of a N_2 carrier gas at high velocity seems to be preferred for the growth of epitaxial layers. Isotherms confined and parallel to the substrate surface help prevent parasitic gas phase reactions, and uniform flow fields allow more uniform mass transfer. The work of Sacilotti et al. [28] showed that more uniform epitaxial layers were deposited in the deposition of InP from $In(CH_3)_3$ and PH_3 in a horizontal reactor when N_2 was used as the carrier gas as compared to H_2. Other problems such as the purity of the N_2 carrier gas and the positive role of H_2 in the deposition chemistry (e.g., reducing carbon incorporation by reaction with methyl radicals), however, must be considered when selecting the carrier gas. From the perspective of gas dynamics in a vertical reactor, the upflow reactor configuration is preferred, since it can more easily provide forced convection dominated flow fields due to the stabilizing density gradient developed in the reactor. It also provides more favorable arrangement for particle rejection. Substrate handling issues related to automation, however, need to be carefully addressed for successful operation.

4. Summary

Temperature profiles in a vertical upflow OMVPE reactor were measured by pure rotational Raman scattering from the carrier gas molecules. It was found that a larger temperature gradient normal to the susceptor surface can be obtained with a higher gas flow velocity, larger aspect ratio, and the use of a N_2 carrier gas. Experimental results also suggested from the perspective of gas dynamics that the upflow reactor geometry with the use of N_2 carrier gas can provide a favorable environment for the epitaxial growth.

Acknowledgements

Authors would like to thank Dr. Z.S. Huang and Dr. A. Zhao for their fruitful discussions. This work is supported in part by KOSEF Grant #96-0300-14-01-3.

References

[1] J.P. Hirtz, M. Razeghi, M. Bonnet and J.P. Duchemin, in GaInAsP Alloy Semiconductors, Ed. T.P. Pearsall (John Wiley & Sons, New York, NY, 1982) ch. 3.
[2] G.B. Stringfellow, Organometallic Vapor-Phase Epitaxy: Theory and Practice (Academic Press, San Diego, CA, 1989).
[3] K.F. Jensen, J. Crystal Growth 98 (1989) 148.
[4] L.J. Giling, J. Electrochem. Soc. 129 (1982) 634.
[5] D.J. Fotiadis, S. Kieda and K.F. Jensen, J. Crystal Growth 102 (1990) 441.
[6] K.F. Jensen, D.I. Fotiadis and T.J. Mountziaris, J. Crystal Growth 107 (1991) 1.
[7] S. Patnaik, R.A. Brown and C.A. Wang, J. Crystal Growth 96 (1989) 153.
[8] G. Wahl, Thin Solid Films 40 (1977) 13.
[9] P. Lee, D. McKenna, D. Kapur and K.F. Jensen, J. Crystal Growth 77 (1986) 120.
[10] C.A. Wang, S.H. Groves, S.C. Palmateer, D.W. Weyburne and R.A. Brown, J. Crystal Growth 77 (1986) 136.
[11] Y.N. Makarov and A.I. Zhmakin, J. Crystal Growth 94 (1989) 537.
[12] A.I. Gurary, G.S. Tompa, A.G. Thompson, R.A. Stall, P.A. Zawadzki and N.E. Schumaker, J. Crystal Growth 145 (1994) 642.
[13] G.S. Tompa, P.A. Zawadzki, K. Moy, M. Mckee, A.G. Thompson, A.I. Gurary, E. Wolak, P. Esherik, W.G. Breiland, G.H. Evans, N. Bulitka, J. Hennessy and C.J.L. Moore, J. Crystal Growth 145 (1994) 655.
[14] C. Houtman, D.B. Graves and K.F. Jensen, J. Electrochem. Soc. 133 (1986) 961.
[15] D.I. Fotiadis, A.M. Kremer, D.R. McKenna and K.F. Jensen, J. Crystal Growth 85 (1987) 154.
[16] S.I. Boldish, J.S. Ciofalo and J.P. Wendt, J. Electron. Mater. 14 (1985) 587.
[17] V.S. Ban, J. Electrochem. Soc. 125 (1978) 317.
[18] L.J. Giling, J. Physique 43 (1982) C5-235.
[19] D.A. Long, Raman Spectroscopy (McGraw-Hill, New York, NY, 1986).
[20] H.W. Schrötter and H.W. Klöckner, in: Raman Spectroscopy of Gases and Liquids, Ed. A. Weber (Springer-Verlag, Berlin, 1979) ch. 4.
[21] M. Koppitz, O. Vestavik, W. Pletschen, A. Mircea, M. Heyen and W. Richter, J. Crystal Growth 68 (1984) 136.
[22] H. Moffat and K.F. Jensen, J. Crystal Growth 77 (1986) 108.
[23] L. Stock and W. Richter, J. Crystal Growth 77 (1986) 144.
[24] J. Van de Ven, G.M.J. Rutten, M.J. Raaijmakers and L.J. Giling, J. Crystal Growth 76 (1986) 352.
[25] D.I. Fotiadis, M. Boekholt, K.F. Jensen and W. Richter, J. Crystal Growth 100 (1990) 577.
[26] Y. Monteil, M.P. Berthet, R. Favre, A. Hariss, J. Bouix, M. Vaille and P. Gibart, J. Crystal Growth 77 (1986) 172.
[27] Y. Monteil, R. Favre, A. Bekkaoui, P. Raffin, J. Bouix, J. Marcillat and P. Dutto, J. Crystal Growth 93 (1988) 270.
[28] M. Sacilotti, A. Mircea and R. Azoulay, J. Crystal Growth 63 (1983) 111.